



Alumina supported nanoruthenium as efficient heterogeneous catalyst for the selective H₂O₂ oxidation of aliphatic and aromatic sulfides to sulfoxides

P. Veerakumar^a, Zong-Zhan Lu^b, M. Velayudham^b, Kuang-Lieh Lu^b, S. Rajagopal^{a,*}

^a Department of Physical Chemistry, School of Chemistry, Madurai Kamaraj University, Madurai, 625 021, India

^b Institute of Chemistry, Academia Sinica, Taipei, 115, Taiwan

ARTICLE INFO

Article history:

Received 12 June 2010

Received in revised form 4 September 2010

Accepted 6 September 2010

Available online 15 September 2010

Keywords:

PVP

γ-Al₂O₃

30% H₂O₂

RuNPs

Sulfides

Sulfoxides

ABSTRACT

Highly stable polyvinylpyrrolidone (PVP) capped ruthenium nanoparticles (RuNPs) supported on γ-Al₂O₃ in CH₃CN serve as efficient heterogeneous catalysts for the H₂O₂ oxidation of sulfides into the corresponding sulfoxides in excellent yields. The synthesized catalyst **I** is well characterized by XRD, HRTEM, BET, H₂ chemisorption, SEM–EDX, AFM, FT-IR, and UV–vis spectral techniques. The catalyst **I** can be recovered and reused for several cycles without loss of any activity.

© 2010 Elsevier B.V. All rights reserved.

1. Introduction

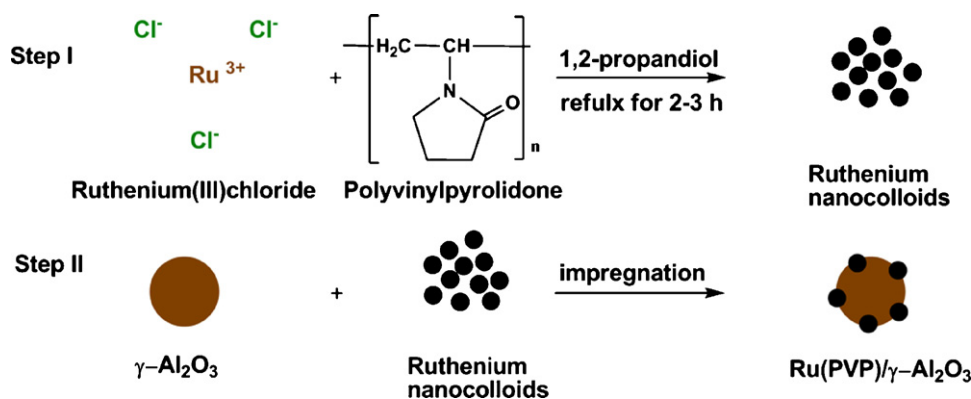
Heterogeneous catalysis has been employed as an important chemical technology because of its inherent operational advantages such as ease of handling, separation, and recovery for the reuse of catalysts [1]. Ruthenium, in the nanoform, is known for the past one decade to show fascinating catalytic activity for the oxidation reactions [2]. Ruthenium is less expensive compared to Au, Pd, Pt, and Rh which have been extensively used as catalysts for organic transformations. [3,4]. Nanocrystalline gamma-phase (γ) alumina is among many polytypes of alumina that find extensive applications as a catalyst and catalytic support [5,6]. The number of ruthenium-catalyst systems used, employing oxygen (or air) as the sole oxidant, is limited. For example, [RuCl₂(*p*-cymene)]₂ complex on carbon [7] and Ru/C [8] have been shown to catalyze the oxidation of alcohols, Ru/CeO₂ [9] and Ru/Al₂O₃ [10,11], for the oxidation of alcohols and amines. Ru-hydroxyapatite (nano-RuHAP) [12] has been used for effective oxidation reactions using NaO₄ as an oxidant. The most useful properties provided by alumina as catalyst support are high surface

area and well defined porosity. Apart from ruthenium, other metal nanocatalysts, e.g., Ag [13], Pd [14], Cu [15], Au [16], Ni [17] and Pt [18] on alumina support were used as the catalysts for oxidation reactions.

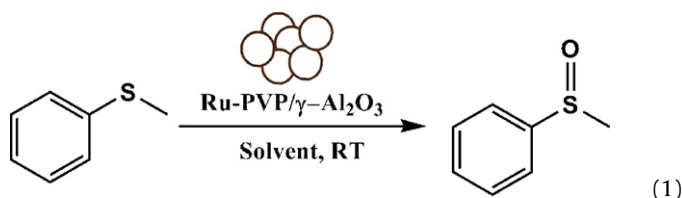
The oxidation of organic sulfides to the corresponding sulfoxides is one of the important functional group transformations in organic synthesis [19]. Organic sulfoxides are also important intermediates for the asymmetric synthesis of biologically active compounds [20]. The oxidation reaction of organic sulfides is also of potential use in the decontamination of toxic chemicals and facile electron transfer reactions [21,22]. The metal-salen complexes (metal = Mn, Cr, Fe, Ru, Co, V and Ti) have extensively been used, particularly in our laboratory, as efficient homogenous catalysts for the selective oxygenation of organic sulfides and sulfoxides [23–28]. Very recently efficient oxidation of sulfides to sulfoxides with H₂O₂ catalyzed by core-shell (SiO₂@WO₄²⁻) nanoparticles has been reported [29]. The uncatalyzed H₂O₂ oxidation of sulfide into sulfoxide or sulfone at room temperature (RT) is a slow reaction [30]. Herein we report a novel and simple method for the oxidative conversion of sulfides to sulfoxides using H₂O₂ as the oxidant and RuNPs loaded on γ-Al₂O₃ as the catalyst **I**, (Ru (PVP)/γ-Al₂O₃). H₂O₂, an environmentally benign oxidant, is frequently used by many researchers. However, H₂O₂ alone has to be used in a controlled manner to reduce the possibility of an over-oxidation reaction. Therefore, there is a need to improve the utility of H₂O₂ for the selective conversion of sulfides to sulfoxides. The title reaction is represented in Eq. (1).

* Corresponding author. Tel.: +91 452 2458246; fax: +91 452 2459105.

E-mail addresses: rajagopalseenivasan@yahoo.com, spveerakumar@gmail.com (S. Rajagopal).



Scheme 1. Two-step process for the synthesis of catalyst I.



2. Experimental

2.1. Materials

$\text{RuCl}_3 \cdot \text{H}_2\text{O}$ (38.0–42.0% Ru basis), 1,2-propanediol, polyvinylpyrrolidone (PVP, Mw ~ 40,000), $\gamma\text{-Al}_2\text{O}_3$, methyl phenyl sulfide (MPS), *para*-substituted phenyl methyl sulfides (*p*-methoxy, *p*-methyl, *p*-fluoro, *p*-chloro, *p*-bromo, and *p*-nitro), diphenyl, diethyl, di-*n*-propyl, di-*n*-butyl, and di-*sec*-butyl sulfide were purchased from Aldrich and used as such. HPLC grade acetonitrile and 30% H_2O_2 were used as received. All the glassware were cleaned with aqua regia (v/v, HCl/HNO_3 , 3:1; caution: aqua regia is very toxic and should be handled carefully!)

2.2. Synthesis of Ru (PVP)/ $\gamma\text{-Al}_2\text{O}_3$ catalyst

Metal colloids dispersed liquid medium can be divided into four categories, solvent-stabilized [31], surfactant-stabilized [32], ligand-stabilized [33] and polymer-stabilized [34]. Metal colloids of the first three categories are usually unstable when they are used as catalysts even when the reaction conducted in ambient conditions. Thus, the polymer-stabilized metal colloids are the most useful catalytic systems for organic transformation. Very stable PVP-capped RuNPs were synthesized by reduction of Ru^{3+} with 1,2-propanediol in the presence of PVP according to Chen et al. [35] Briefly, RuCl_3 (0.1434 g, 5.25×10^{-4} M), and PVP (0.5828 g, 5.25×10^{-3} M, as monomeric unit) were dissolved in 1,2-propanediol (100 mL) under stirring to form a dark red solution and refluxed. The color of the solution changed from dark red to yellow and then turned to deep green and finally to dark brown. The dark brown colored solution was then left to cool to room temperature. Scheme 1 illustrates the two-step process that we have used for the synthesis of the RuNPs supported on the alumina: (1) synthesis of the ruthenium colloids, and (2) impregnation of the RuNPs onto the alumina nano surface using PVP as the stabilizer. The 1,2-propanediol was removed later by diluting the suspension with 450 mL of 0.3 M NaNO_3 aqueous solution. The black solid was collected by filtration, washed with distilled water to remove the Na^+ and Cl^- ions, dried under vacuum at RT and calcinated at 500°C for 8 h and stored in a closed con-

tainer. The details of the synthesis of the catalyst I are given in Scheme 1.

The catalyst support, $\gamma\text{-Al}_2\text{O}_3$, was dried at 120°C overnight prior to impregnation and surface area $>40\text{ m}^2/\text{g}$ (BET) is the property which makes $\gamma\text{-Al}_2\text{O}_3$ appealing as a catalyst support. The γ -alumina supplied by Sigma–Aldrich with an average particle size of $<50\text{ nm}$ (TEM) is used as the support in this study.

2.3. Characterization

Powder X-ray diffraction (XRD) patterns were recorded using a XPERT-PRO diffractometer operated at a voltage of 40 kV and a current of 30 mA with $\text{Cu K}\alpha$ radiation ($\lambda = 1.54060\text{ \AA}$). High resolution transmission electron microscopy (HRTEM) and selected area electron diffraction (SAED) patterns were performed using a JEOL 3011, 300 kV instrument with a UHR pole piece. The nitrogen adsorption/desorption was performed by using a Micromeritics ASAP 2010 sorptometer for high-resolution low surface area studies. The same apparatus was used to perform H_2 chemisorption measurements. Detailed measurements of surface area were determined from nitrogen adsorption isotherm by the Brunauer–Emmett–Teller (BET) method and determination of the pore size distribution from adsorption branch by the Barrett–Joyner–Halenda (BJH) method. SEM–EDX observations were carried out on a Hitachi S-3400N electron microscope. The energy dispersive X-ray analysis (Thermo SuperDry II) is used to carry out semi-quantitative elemental analysis of the samples. EDX observations were carried out by a cathodoluminescence detector. Ultraviolet–visible absorption spectra were recorded using a SPECORD S100 diode-array spectrophotometer. FT-IR spectra were recorded using 8400S Shimadzu FT-IR spectrometer in the region of $4000\text{--}400\text{ cm}^{-1}$ with a spectral resolution of 2 cm^{-1} using dry KBr at room temperature. Atomic force microscopy (AFM) (APE Research nanotechnology, AFM A100 SGS), working at 100 kV, was used to measure the size of nanoparticles. The samples for AFM measurements were prepared by evaporating a drop of the dilute aliquot solution on a thin glass plate. ^1H NMR data for the sulfoxides were acquired on a Bruker 300 MHz NMR spectrometer with CDCl_3 as the solvent. GC analyses were carried out using a Shimadzu 17 A model capillary gas chromatography (SE-30 10%; carbowase and ZB-55%, with FID detector).

2.4. Selective oxidation

The general procedure for the sulfoxidation reaction is as follows: Catalyst I (1 wt%, 0.5–2.0 mmol) and sulfide (1.0 mmol) were dissolved in CH_3CN (3 mL) at 298 K. To this mixture, 30% H_2O_2 (1.0 mmol) was added dropwise slowly. The mixture was stirred

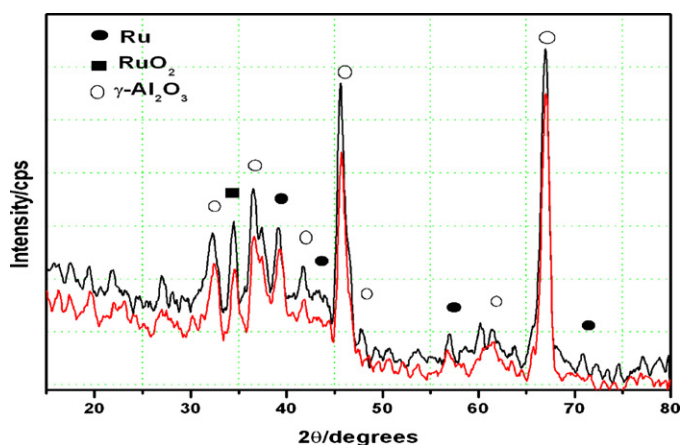


Fig. 1. The XRD patterns of the catalyst I. The catalyst was calcinated at 500 °C in air for 8 h. Fresh catalyst (black line), and used catalyst (red line). (●), Ru; (■), RuO₂; (○), (-)Al₂O₃. (For interpretation of the references to color in this figure legend, the reader is referred to the web version of the article.)

for 1–2 h at room temperature. The resulting solution was diluted with CHCl₃, washed initially with water and then with saturated brine solution. The organic layer was dried over anhydrous MgSO₄, filtered and concentrated under reduced pressure. The crude product was purified by flash column chromatography on silica gel using petroleum ether and ethyl acetate (2:1) as eluent. The solvent was evaporated and the product was analyzed using ¹H NMR and FT-IR techniques.

3. Results and discussion

3.1. XRD results

The X-ray diffraction pattern of the catalyst I is shown in Fig. 1. For the metallic ruthenium, the diffraction peak is around $2\theta = 44^\circ$ which is exactly consistent with the d value (2.11 Å) of standard ruthenium metal data file (JCPDS No. 06-0663). The pattern of the

catalyst I (Fig. 1) containing reflections from γ -Al₂O₃, Ru, and RuO₂ were detected by XRD. Fig. 1 also indicates a very little aggregation on the catalyst surface. Minor ruthenium reflections peaks emerging from catalyst I indicate that Ru forms very small particles dispersed on the support [36]. The Ru colloids showed a diffuse peak which was separated into three independent peaks located at $2\theta = 38.5^\circ$, 42.8° and 44° stand for Ru (1 0 0), Ru (0 0 2) and Ru (1 0 1), respectively [37].

The average crystal size of the RuNPs calculated by the Scherrer formula is in agreement with the average diameter (5–6 nm) determined by HRTEM. (*vide infra*).

3.2. HRTEM results

Representative HRTEM images of the catalyst I (Fig. 2a and b) show the presence of numerous dark and well-dispersed RuNPs on the alumina support. These dark spots correspond to the RuNPs. The individual RuNPs have clear edge and are quite uniform in size as shown in Fig. 2c. The RuNPs are crystalline and the observed lattice fringes are shown in Fig. 2d. The average diameter of RuNPs estimated from the Gaussian fit of the particle size distribution histograms is about 5–6 nm. SAED (Selective Area Electron Diffraction) analysis also confirmed that the RuNPs have an average diameter of about 5–6 nm.

At low magnification all particles appear as smooth-surfaced and perfect spheres (Fig. 2a). At higher magnification, the particles are single crystals exhibiting lattice fringes characteristic of Ru⁰. The electron diffraction pattern of the representative ruthenium nanoparticle is also shown in Fig. 2d; it exhibits bright spot with rings with the d -spacings of hcp ruthenium metal. Considerable broadening of the diffraction rings suggests that the particles are very small and of high crystallinity. These results are in good agreement with the corresponding XRD data. When high-energy X-ray diffraction is used for the characterization of RuNPs it is realized that the nanoparticles are only 5 nm in size and are heavily disordered [38]. Calcination at 500 °C for 8 h caused some broadening of the particle size distribution and the particles had crystal faces with no evidence of any amorphous surface layer (Fig. 2d). Bedford

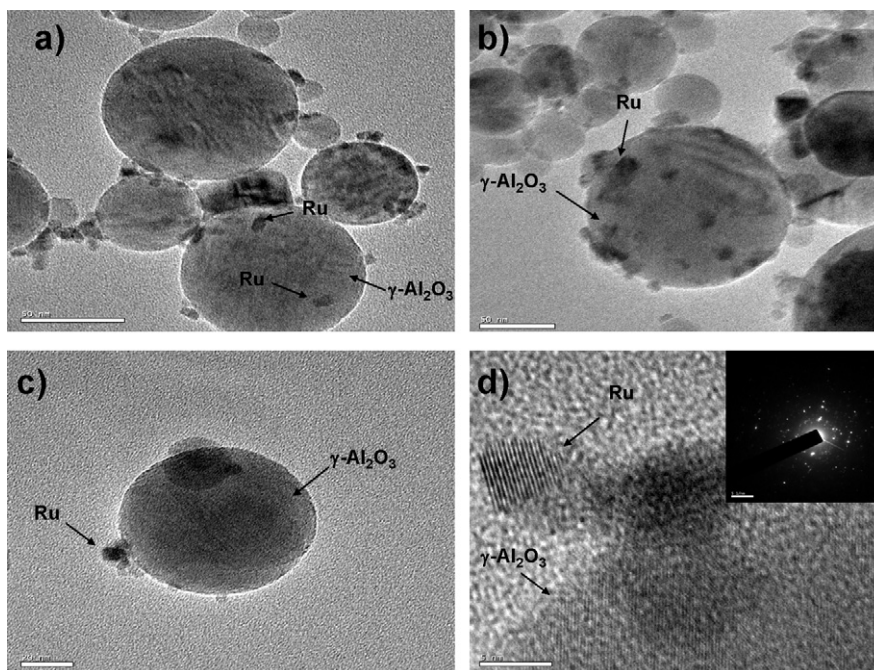


Fig. 2. HRTEM images of ruthenium catalyst I. (a), (b), (c), and (d) correspond to the different images and electron diffraction pattern of the representative ruthenium nanoparticle is also shown in inset (d). The bars represent (a, b) 50 nm, (c) 20 nm, and (d) 5 nm.

Table 1
Physicochemical properties of the γ -Al₂O₃ and catalyst I.

Sample	Ru content (wt%)	BET surface area (m ² /g)	Langmuir surface area (m ² /g)	t-plot micropore area (m ² /g)	Average pore diameter (nm)	Pore volume (cm ³ /g)
γ -Al ₂ O ₃	–	26.5	42.4	0.19	33	0.13
Catalyst I	1.0	24.2	40.0	0.14	20	0.05

et al. [39] showed, by calcination at higher temperatures, 600 and 700 °C, significant broadening of the particle shape with increasing particle size from round ones (small particles) to flat, elongated ones (large particles). It has high thermal stability up to 700 °C of small RuNPs which has already been reported [40].

3.3. BET surface area studies

The N₂ adsorption and desorption isotherms for γ -Al₂O₃ and catalyst I were measured at 77 K. Prior to the adsorption measurement, the samples were pretreated under helium gas flow at 300 °C for 4 h. Total surface areas were calculated according to the BET and Langmuir methods [41]. Alumina exhibited a Brunauer–Emmett–Teller (BET) surface area of 26.5 m²/g, including micropore area of 0.19 m²/g and external surface area of 29.2 m²/g. The catalyst I gave a BET surface area of 24.2 m²/g, average micropore area of 0.14 m²/g and external surface area of 26.3 m²/g. The decrease in surface area is mainly due to the reduction of micropore surface area. The results help us to conclude that the RuNPs were

impregnated on the surface of the γ -Al₂O₃. The RuNPs were well dispersed on the outside surface and no obvious aggregation was observed, whereas unsupported RuNPs were likely to aggregate immediately.

From the measurements, the BET surface area, Langmuir surface area, pore volume and average pore diameter were calculated and the data are given in Table 1.

The change in textural property of γ -Al₂O₃ and RuNPs impregnated on γ -Al₂O₃ (catalyst I) are given in the supporting information. A sharp inflection of the adsorption and desorption isotherms, in particular around $P/P_0 = 0.9712$ (for N₂ at 77 K), indicates a forced closure of the hysteresis loop. In Fig. 3a the inset figure shows the details of the isotherm in the P/P_0 range 0.8–1.0 (dotted square) emphasizing the TSE (tensile strength effect) at $P/P_0 = 0.97$. The $(4V/A)$ term used in the estimation of pore average sizes corresponds to the assumed cylindrical model of pores. However, this assumption of cylindrical model of pores is also cited in BJH estimates of pore volume and surface area distributions. Fig. 3b shows the adsorption and desorption isotherm value of catalyst I at $P/P_0 = 0.9711$. However, pores with diameters smaller than 4 nm show no hysteresis and are completely filled and emptied at similar pressures, resulting in a reversible adsorption and desorption isotherm [42]. The results may point to localization of the RuNPs mainly at the outer surface of the γ -Al₂O₃ and only some of them may be present inside the γ -Al₂O₃ pores. The average pore diameter, pore volume and surface area of the γ -Al₂O₃ decrease after impregnation with RuNPs (Table 1). Okal et al. [43] reported that the impregnation of γ -Al₂O₃ with an aqueous solution of RuCl₃ caused a 25% decrease in BET surface area and some drop of the pore volume. Mieth and Schwarz [44] pointed out that the partial dissolution of the support during impregnation may have significant consequences on the catalyst activity. Similar effect was observed in other systems such as Pd/Al₂O₃ [45] and Pt/Al₂O₃ [46]. The adsorption studies help us to conclude that due to impregnation of RuNPs on γ -Al₂O₃ the surface area, pore diameter and pore volume of catalyst I decreased.

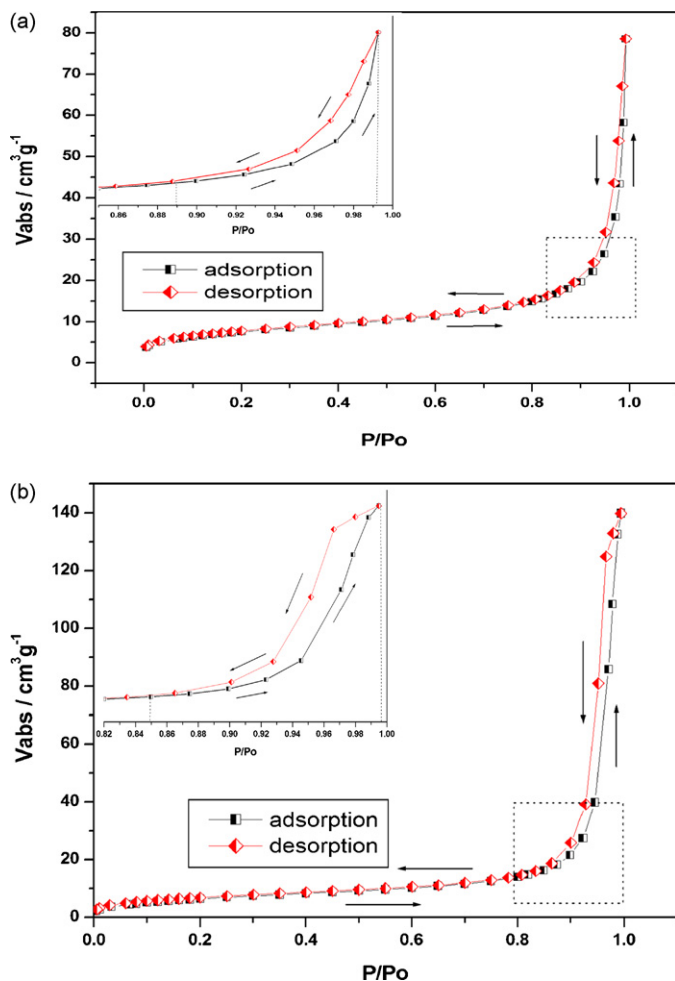


Fig. 3. Adsorption–desorption isotherm for (a) γ -Al₂O₃ and (b) catalyst I.

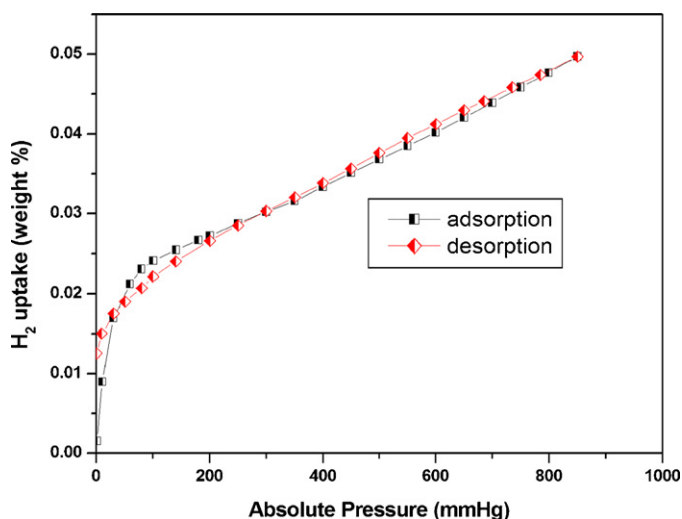


Fig. 4. Hydrogen chemisorption isotherm of catalyst I.

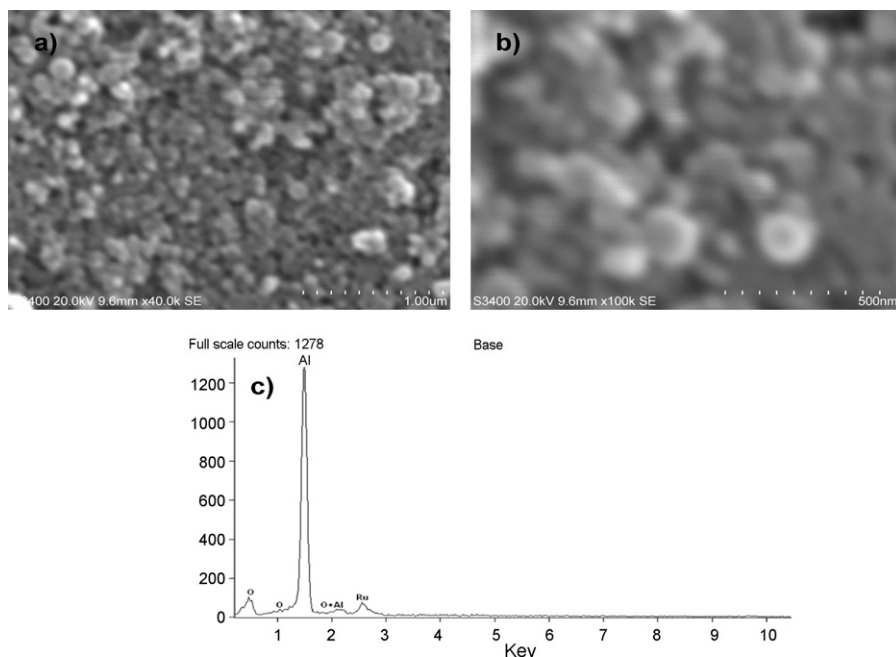


Fig. 5. SEM pictures of catalyst I: (a) 40 K \times magnification, (b) 100 K \times magnification and (c) EDX analysis of catalyst I.

3.4. Hydrogen chemisorption studies

Fig. 4 presents the hydrogen chemisorption on catalyst I carried out at 77 K using Micromeritics 2020 equipment with use of glass volumetric adsorption system described elsewhere [47]. This study provides hydrogen/metal (H/M) data. (H/M is the ratio of the number of adsorbed hydrogen atoms to the total number of metal atoms multiplied by 100%.) Each measurement was performed three times and the average value $H/M = 1:1$ was used. The total amount of adsorbed hydrogen was obtained by extrapolating the linear high-pressure part of the isotherm to zero pressure. H_2 chemisorption at 77 K is helpful to determine the percent dispersion and average Ru particle size to be 17% and 5.1 nm respectively. The equilibrium adsorption measurements were made for equilibrium pressures of 0–850 mm Hg range. Average RuNPs size was estimated using the relation $l(\text{chem}) = 5/Sd$, where S is the metal surface area and d is the density of ruthenium [48,49].

The reversible hydrogen isotherms (Fig. 4) show a linear dependence on pressure in the 200–850 mm Hg range but the uptake decreased slowly at 200 mm Hg (see supporting information). Sayari et al. [50] found that at room temperature reversible H_2 chemisorption occurs in appreciable amounts on the Ru crystallites with sizes within the limited range of 5–6 nm. Zupanc et al. [51] explained this finding by a modification in the surface energetics of the Ru crystallites with the change of their size. However, only very small change in the mean size of RuNPs was detected by the hydrogen chemisorption.

3.5. SEM–EDX observations

SEM–EDX shows typical results of catalyst I deposited on a carbon strip by means of SEM. Fig. 5a represents the view of the sample at 40k \times magnification which stands for examining the area of $9.6 \times 9.6 \text{ mm}^2$ surface. These objects consist of tiny particles, confirmed by SEM results.

Analysis through energy dispersive X-ray (EDX) spectrometers confirmed the presence of elemental ruthenium and aluminum signals from the catalyst I (Fig. 5). The vertical axis displays the number of X-ray counts whilst the horizontal axis displays energy in keV.

Identification lines for the major emission energies of Al metal from the catalyst I are displayed and these correspond with peaks in the spectrum, thus giving confidence that ruthenium has been correctly identified (see supporting information).

3.6. UV–vis absorption spectral data

UV–vis absorption spectroscopy was also used to establish the complete reduction of Ru^{3+} to Ru^0 state [52,53]. The Ru^{3+} is mixed with PVP in 1,2-propanediol and heated to the temperatures indicated in Scheme 2.

Ru^{3+} (dark red) was reduced, step-by-step, to Ru^0 (dark brown) during the reaction: (a) the reaction mixture at the beginning of the reaction; (b) reaction solution obtained at approximately 20 min of the reaction; (c) at approximately 30 min (d and e), at 50–90 min; (f) at the end of the reaction. The UV–vis absorption spectra of the solutions are displayed in Fig. 6 and color changes with the change of temperature is shown in Scheme 2.

One of the well-known reduction methods for the preparation of metal colloid is by employing 1,2-propanediol as a solvent and reducing agent, and the polymer like PVP as the stabilizing agent.

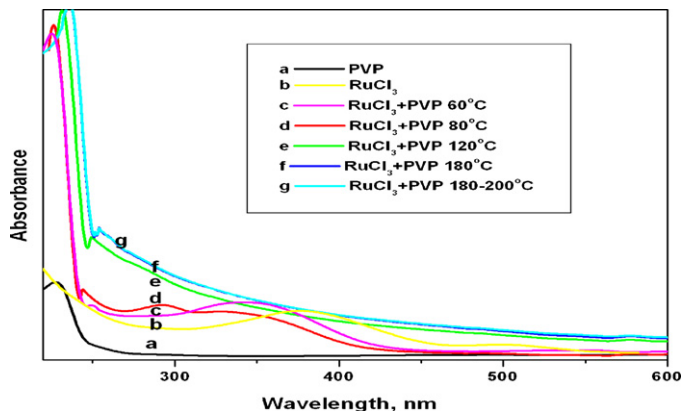
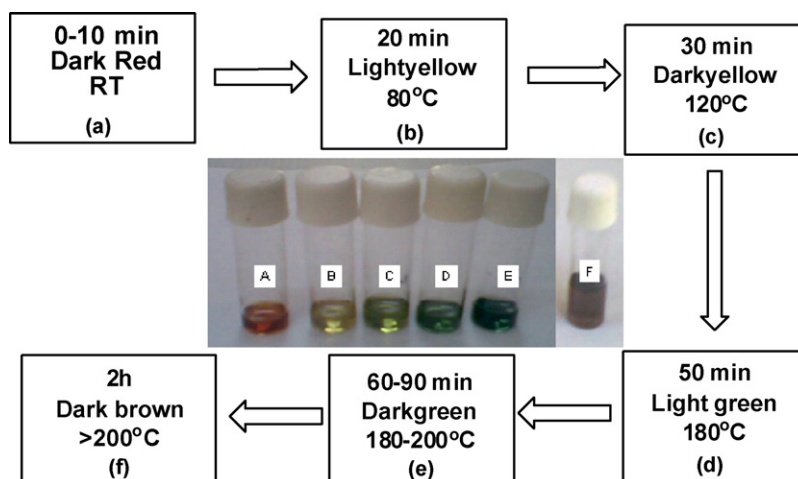


Fig. 6. UV–vis absorption spectra of the PVP–Ru in a 1,2-propanediol solution at different stages.



Scheme 2. Color changes of the reaction solution during the course of the Ru nanocolloids formation with 1,2-propanediol taken as solvent.

Table 2

Relationship between the oxidation states of Ru in the Ru-PVP in 1,2-propanediol with the absorbance data.

Oxidation state	Temp (°C)	Color	Wavelength (nm)
Ru ³⁺	RT	Dark red	391
Ru ²⁺	80–120	Yellow	345
Ru ⁺	120–180	Green	328
Ru ⁰	>200	Dark brown	No characteristic peak

The standard reduction potential of Ru³⁺ to Ru⁰ is relatively high ($E^0 = 0.3862$ V) [54]. The redox properties of 1,2-propanediol is similar to 1,2-ethanediol [55] but it is less toxic [56].

The UV–vis spectrum of the freshly prepared Ru³⁺ solution in 1,2-propanediol exhibited a broad absorption with maximum at 391 nm. It is well known that colloidal dispersion of metals exhibit broad regions of absorption in the UV–vis range. These are due to the excitation of plasma resonances or interband transitions, and they are thus a very characteristic property of the metallic nature of the particles (Fig. 6b). This peak is shifted to a shorter wavelength, 345 nm, after 20 min of reduction (Fig. 6c). At this reduction time the solution turned to light yellow color. The intensity of the peak decreases at 328 nm and the solution turned dark green by further heating. After about 110 min, the absorption peak disappeared completely, which indicated that Ru³⁺ was entirely reduced to Ru⁰ (Fig. 6f and g). The increasing scattering absorbance at wavelengths between 300 and 800 nm with time revealed the formation of ruthenium colloids [57]. Each color change represents a change in the oxidation state of ruthenium and reduction takes place stepwise from Ru³⁺ state to Ru⁰ state and the details are collected in Table 2.

3.7. AFM analysis

AFM provides real topographical image of sample surface. Since ruthenium nanocatalysts exhibit physical properties different from bulk ruthenium and the properties largely dependent on their size and structure, a good structural characterization becomes possible. A good dispersion of the nanoparticles is possible to image them individually using AFM. Further, this technique enables measuring the size of the particle, considering the particle height rather than its width because the particle may be distorted by the AFM tip geometry. Fig. 7 provides three-dimensional structural information, which is not available with conventional light-scattering measurements. Fig. 7a and b shows three-dimensional overview of the fresh catalyst I in a scan size of $1.7 \times 1.7 \mu\text{m}$.

The nanoparticles have an average size of 50–100 nm and are separated from each other. The particle size of nanoruthenium was determined using HRTEM as shown in Fig. 2.

3.8. FT-IR analysis

The γ -alumina is chemically inert in 1,2-propanediol under the conditions used in this study and thus used as a support for Ru catalyst. The catalyst I is characterized using FT-IR spectroscopy and the spectrum is shown in Fig. 8.

The FT-IR fingerprints of the PVP indicate that the polymer is present on the surface of the RuNPs serving as a good stabilizing agent. Compared to the spectrum of PVP, the resonance peak of C=O of PVP coordinated to RuNPs was shifted from 1656 cm^{-1} to 1644 cm^{-1} while the C–N peaks at (1014 cm^{-1} and 1074 cm^{-1}) were not changed. These changes suggest that the coordination of nitrogen-containing heterocyclic ring of the PVP to the RuNPs sur-

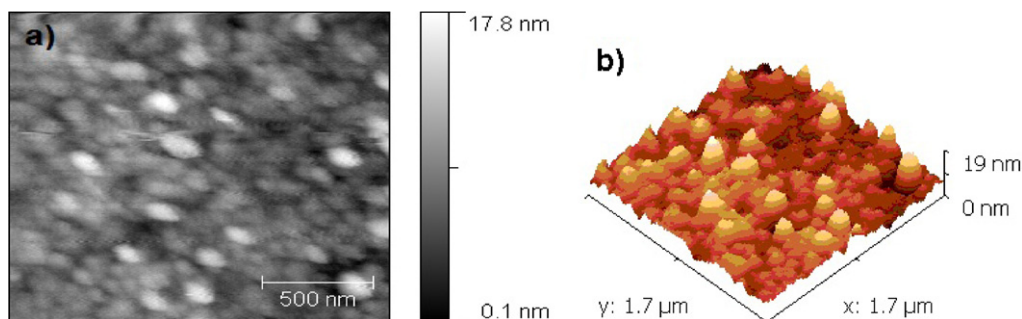
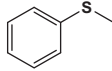
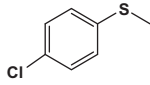
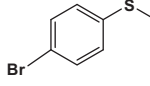
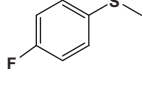
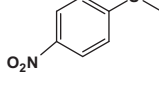
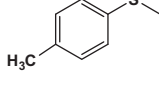
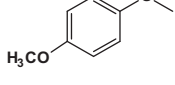
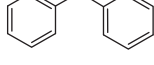
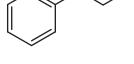
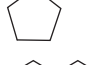
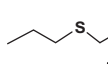
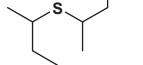
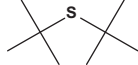
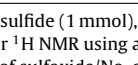


Fig. 7. (a) AFM image of catalyst I in 2D and (b) the 3D representation.

Table 3
Oxidation of various sulfides H₂O₂ catalyzed catalyst I^a.

Entry	Substrate	Time (min)	Conversion (%) ^b	Yield (%) ^{b,c}	Selectivity (%) ^{b,c}
1		120	100	98, 92 ^b , 98 ^c	98
2		150	98	96	95
3		150	98	97	98
4		150	99	96	96
5		180	99	90	95
6		120	98	92	98
3		100	99	97	99
8 ^f		75	99	99	99
9		110	99	92	97
10		100	95	96	94
11		100	>98	100	99
12		100	>98	100	98
13		100	>97	100	99
14		100	>97	100	97

^a Reaction conditions: sulfide (1 mmol), 30% H₂O₂ (1 mmol), catalyst I (1 wt%, 0.5–2 mmol), CH₃CN (3 ml).

^b Determined by GC or ¹H NMR using an internal standard technique on the crude reaction mixture.

^c Yield = No. of moles of sulfoxide/No. of moles of sulfide; Selectivity = Sulfoxide/(Sulfoxide + Sulfone).

^{d,e} The catalyst is reused repeatedly.

^f MeOH was used (70% yield in CH₃CN medium).

face may be weaker compared to the carbonyl group [34]. Such PVP coordination to the surface of the RuNPs was also proposed by Bonet et al. [58] the spectrum also exhibits an O–H stretching mode, associated with water and hydroxide species centered at $\sim 3470\text{ cm}^{-1}$ and $\sim 1620\text{ cm}^{-1}$ respectively. Though the signal obtained for the FT-IR spectrum is predominantly from the RuNPs there is some contribution from the surface of γ -alumina as shown in Fig. 8.

3.9. Selective oxidation of sulfides to sulfoxides

In this study, 14 organic sulfides are oxidized to sulfoxides by using H₂O₂ and catalyst I (Table 3).

After the completion of the reaction, the catalyst was extracted with CHCl₃. The oxidation process was repeated for three consecutive cycles with little loss of activity (entry 1). The data collected in Table 3 show that the rate of oxidation of aromatic sulfides varied

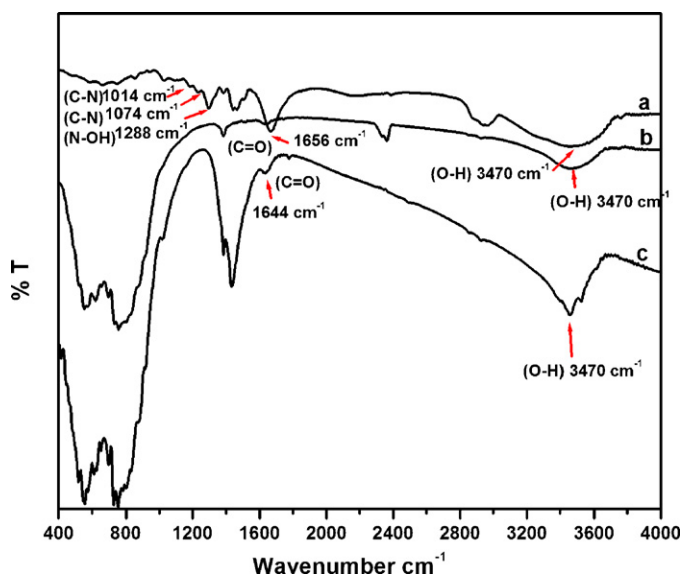


Fig. 8. FT-IR spectra of (a) PVP (b) $-\text{Al}_2\text{O}_3$ and (c) catalyst **I** after treatment at 500°C .

with the nature of substituents on the phenyl ring (entries 2–7). The presence of electron withdrawing substituents on the phenyl ring required slightly longer reaction times when compared to electron donating substituents. Selectivity towards the formation of sulfoxide is higher than 90% in all cases and in most of the cases it is close to 100%. The other product expected is the corresponding sulfone but the yield of sulfone is negligible here. However, with increase in time and H_2O_2 , the formation of sulfone (i.e. overoxidation) has been observed. As far as diphenyl sulfide (DPS) is concerned MeOH seems to be better solvent than CH_3CN . The alkyl sulfides are more reactive than aryl sulfides and the reaction is little sensitive to steric effect. The values of selectivity for the obtained products are presented in Table 3. Notably, the use of catalyst **I** at 1 wt% resulted in the quantitative conversion of sulfides to the corresponding sulfoxides with 1 mmol of 30% H_2O_2 .

3.10. Product analysis

The H_2O_2 oxidation of sulfides in the presence of the catalyst **I** was monitored via ^1H NMR to identify the products of the reaction. The ^1H NMR spectra for the products obtained during the course of the reaction (entry 1, 5, 8, 10 and 13 in Table 3) are shown in Figs. S4–S15 (see supporting information). CDCl_3 is used as the solvent and TMS as an internal standard. The peak appeared as a singlet at δ 2.73 ppm corresponds to methyl proton. The aromatic region is also informative as the aromatic protons of sulfoxide appear as multiplets centered at δ values 7.4–7.6 ppm [59–63]. The FT-IR spectrum of the product obtained from the oxidation of MPS shows $\text{S}=\text{O}$ stretching frequency at 1043 cm^{-1} and no stretching frequency at 1150 cm^{-1} corresponding to the formation of sulfone is seen. The interesting aspect of this work is that the substrate to H_2O_2 molar ratio of 1:1 was sufficient enough to give 98% conversion within 2 h. Increasing the amount of oxidant to 2:1 (oxidant:substrate) molar ratio causes the formation of a mixture of sulfoxide and sulfones which is confirmed using ^1H NMR and FT-IR spectroscopy (see supporting information). The aqueous layer containing the catalyst was washed with acetone three times, dried in vacuum and preserved for the next run to check their catalytic activity. This product analysis study demonstrates that sulfoxide is the only product formed under the present reaction conditions.

Table 4

Oxidation of MPS by H_2O_2 in the presence of catalyst **I**^a.

Entry	Solvent	Conversion (%) ^b	Yield (%) ^{b,c}	Selectivity (%) ^d
1	–	80	52	86
2	$\text{H}_2\text{O}:\text{CH}_3\text{CN}$	80	75	73
3	MeOH	90	82	80
4	EtOH	95	85	85
5	CH_3CN	98	97	98
6	CHCl_3	72	70	80
7	CH_2Cl_2	75	60	85
8	1,4-Dioxane	88	71	86
9	MeOH	99	98	98 ^e

^a Reaction conditions: 3 mL of solvent; 1.0 mmol of MPS; 1 mmol, H_2O_2 ; 0.5 mmol (catalyst **I**); RT with stirring.

^b Determined by GC on the crude reaction mixture.

^c Yield = No. of moles of sulfoxide/No. of moles of sulfide.

^d Selectivity = Sulfoxide/(Sulfoxide + Sulfone).

^e The substrate used was DPS.

3.11. Influence of different solvents with H_2O_2

We first investigated the oxidation reaction with MPS as model substrate by using 30% H_2O_2 (1.0 mmol) as an oxidant. To a solution of 3 mL of MPS (1.0 mmol) and catalyst **I** (1.0 mmol) taken in a solvent (the reaction was carried out in different solvents) the oxidant was added at room temperature. The results given in Table 4 show that the reaction is sensitive to the change of solvent.

Generally sulfides are insoluble in water, but when a mixed solvent ($\text{H}_2\text{O}:\text{CH}_3\text{CN}$) 1:1 (v/v) is used for oxidation the yield is 75%. As far as the oxidation of MPS is concerned CH_3CN is the best solvent. On the other hand, CH_3OH seems to be the better solvent for the oxidation of DPS and it provides the highest yield (99%) and selectivity is 98%. The data collected in Table 4 show that of all the solvents, the selectivity and yields are better in CH_3CN but lower in the mixed solvent $\text{H}_2\text{O}:\text{CH}_3\text{CN}$ (1:1) because the substrates are poorly soluble in water specifically.

3.12. Influence of reaction time with MPS

The influence of the reaction time was investigated with catalyst **I** and MPS as the substrate at RT and the results were summarized in Table 5.

Initially the oxidation reaction was slow till 60 min but the reaction is completed in 120 min (Table 5). When the progress of the oxidation reaction was monitored for 30 min, the yield was 60% but the maximum yield is obtained in 120 min. But the increase in the selectivity is also significant, from 85% to 98%, compared with the results obtained in 30 min (Table 5, entry 1 vs. entry 4). If the reaction time is increased to 150 min there is no change in selectivity as well as in yield.

Table 5

Influence of the reaction time with MPS^a.

Entry	Time (min)	Conversion (%) ^b	Yield (%) ^{b,c}	Selectivity (%) ^d
1	30	73	60	85
2	60	89	70	90
3	90	92	85	95
4	120	98	98	98
5	150	98	98	98

^a Reaction conditions: 3 mL of solvent; 1.0 mmol of MPS; 1 mmol, H_2O_2 ; 0.5 mmol (catalyst **I**); RT with stirring.

^b Determined by GC on the crude reaction mixture.

^c Yield = No. of moles of sulfoxide/No. of moles of sulfide.

^d Selectivity = sulfoxide/(sulfoxide + sulfone).

Table 6
Oxidation of MPS using 30% H₂O₂ using different catalysts.

Catalyst ^a	Size (nm)	Mol. (%)	Time (h)	Solvent	Conversion (%)	Yield (%)
LDH-WO ₄ ²⁻ [64]	–	4.4	0.5	H ₂ O	94	88
SiO ₂ @WO ₄ ²⁻ [29]	50–60	2.0	1.5	CH ₂ Cl ₂ :CH ₃ OH	100	82
WO ₃ /MCM-48 [65]	30–100	1.0	4.0	CH ₃ OH	100	100
Nanobiocatalyst [66]	90	5	10 min	–	>99%	>99%
TiO ₂ [62]	6–8	1.25	3.0	CH ₃ CN	100	99
γ-Al ₂ O ₃	<50	0.5	5.0	CH ₃ CN	60	50 ^b
Catalyst I	5–6	0.5	2.0	CH ₃ CN	100	98 ^c
RuCl ₃	–	0.5	5.0	CH ₃ CN	50	Trace ^d

^aReferences.

^{b,c,d}Reaction conditions as exemplified in the experimental procedure.

3.13. Comparison with other catalyst systems

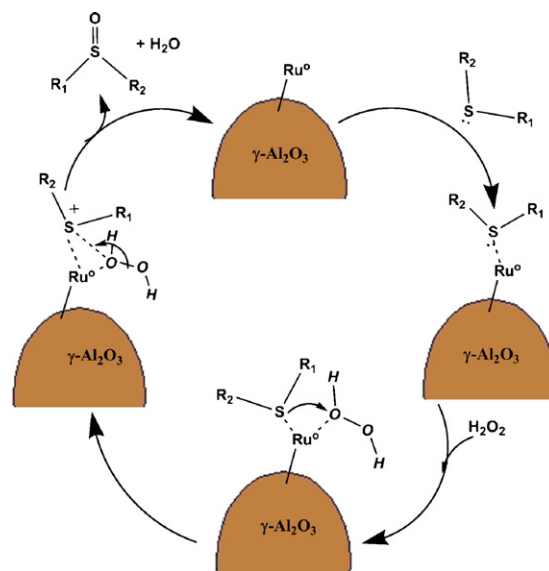
In order to evaluate the efficiency of the catalyst, we have compiled the data available on the H₂O₂ oxidation of MPS in the presence of other catalysts in Table 6. It is clear from the data collected in Table 6 that although the yields are similar, and mol% and the size of catalyst I used in the present case are smallest, the selectivity is better than the other systems, i.e., metal nanoparticles are very attractive catalysts compared to bulk catalytic materials due to their high surface-to-volume ratio. The additional advantage with the present system is that the reaction is conducted at room temperature.

To investigate the effect of size on the catalytic activity, different supported catalysts used for the oxidation of organic sulfides are collected in Table 6. In the present work when catalyst I is used for the oxidation of MPS (as illustrated in Table 3) the reaction is carried out using 0.5 mol% of catalyst I and 1.0 mmol of 30% H₂O₂. The data in Table 6 clearly indicate that the catalyst I has the smallest size but exhibits comparable efficiency and selectivity with SiO₂@WO₄²⁻ [29] and nanocatalyst systems [64–66]. The novelty of this catalyst is that less quantity of catalyst (0.5 mol%) is needed during the sulfoxidation reaction compared to other catalysts (Table 6). Therefore, the catalytic activity is influenced by the nature and size of the nanocatalyst. Thus, ruthenium catalyst (0.5 mol%) in combination with H₂O₂ provided the complete conversion of MPS to MPSO (98% yield), indicating a very good catalytic performance in sulfoxidation reactions. The major problem with the nanobiocatalyst [66] (chloroperoxidase-coated magnetic nanoparticles) is the unsatisfied catalyst stability during operation and the recycling process and the dramatically reduced activity in comparison with catalyst I.

3.14. Mechanism for the oxidation of organic sulfides to sulfoxides

Generally, thiols (–SH) interact strongly with RuNPs [67]. Here we presume that organic sulfides also bind fairly well with Ru surface. A possible reaction mechanism for the H₂O₂ oxidation of sulfides to sulfoxides using catalyst I is proposed in Scheme 3.

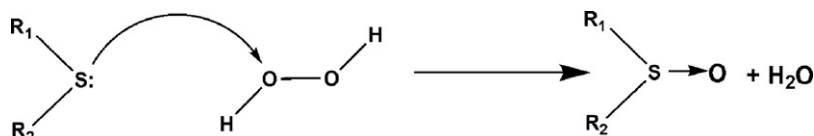
Initially, the sulfur atom of the substrate is likely to attach with the surface of the ruthenium nanoparticles. It is proposed that the interaction between the metal and sulfur is due to metal-to-sulfur charge transfer as the result of thiol–metal bonds at the surface of



Scheme 3. Mechanism for the oxidation of sulfides using catalyst I in CH₃CN.

the particles [68]. It is known that organic sulfides are oxidised by H₂O₂ in a heterolytic process involving the nucleophilic attack of the sulfur atom on the oxygen according to Scheme 4.

The rate of the oxidation of substrates increases with the increased nucleophilicity on the sulfur atom. The oxygen atoms of the H₂O₂ molecule bound on the surface of Ru(0) can interact with sulfide to form an intermediate which readily forms the corresponding sulfoxide and water as the products. Aqueous H₂O₂ is an ideal oxidant owing to its high effective-oxygen content, cleanliness (it produces only water as by-product), and enough safety in storage and operation. Therefore, the importance of H₂O₂ as a “green” oxidizing agent has grown considerably. The progress of the reaction is monitored using TLC and yield of products analyzed by using GC method. Also, the catalyst I was reused up to three times (entry 1 in Table 3) and the catalytic activity decreased only slightly.



Scheme 4. Nucleophilic attack of the sulfur to oxygen atom of H₂O₂.

4. Conclusions

This work provides important insight into the heterogeneous catalysis on the H₂O₂ oxidation of sulfides in the presence of catalyst I, which is one of the most convenient, cheap and green methods for the synthesis of various sulfoxides. The vital role of catalyst is surface binding and the surface binding facilitates the interaction of substrate (thioether) with the oxidant (H₂O₂) resulting in the efficient formation of the selective oxidized products. The synthesized catalyst I was characterized using XRD, HRTEM, BET, H₂ chemisorption, SEM–EDX, AFM, FT-IR, and UV–vis spectral techniques and the characterization of products was done by ¹H NMR, FT-IR, and GC analysis. This nanocatalyst may prove useful in the development of selective oxidation catalyst for the oxidation of other organic substrates.

Acknowledgements

The authors thank UGC for a JRF position under Meritorious Fellowship Scheme and DST for the financial support.

Appendix A. Supplementary data

Supplementary data associated with this article can be found, in the online version, at doi:10.1016/j.molcata.2010.09.008.

References

- [1] A.L. Nuzhdin, D.N. Dymbtsev, V.P. Fedin, G.A. Bukhtiyarova, *Dalton Trans.* (2009) 10481–10485.
- [2] J.M. Basset, J.P. Candy, C.C. Santini, in: M. Beller, C. Bolm (Eds.), *Transition Metals for Organic Synthesis*, 2, Wiley-VCH, Weinheim, 1998, p. 387.
- [3] K. Yamaguchi, N. Mizuno, *Angew. Chem. Int. Ed.* 42 (2003) 1480–1483.
- [4] Y. Na, S. Park, S.B. Han, H. Han, S. Ko, S. Chang, *J. Am. Chem. Soc.* 126 (2004) 250–258.
- [5] B. Tang, J. Ge, L. Zhuo, G. Wang, J. Niu, Z. Shi, Y. Dong, *Eur. J. Inorg. Chem.* (2005) 4366–4369.
- [6] L.J. Alvarez, L.E. Leon, J.F. Sam, M.J. Capitan, J.A. Odriozola, *J. Phys. Chem.* 99 (1995) 17872–17876.
- [7] E. Choi, C. Lee, Y. Na, S. Chang, *Org. Lett.* 4 (2002) 2369–2371.
- [8] S. Mori, M. Takubo, K. Makida, T. Yanase, S. Aoyagi, T. Maegawa, Y. Monguchi, H. Sajiki, *Chem. Commun.* (2009) 5159–5161.
- [9] F. Vocanson, Y.P. Guo, J.L. Namy, H.B. Kagan, *Synth. Commun.* 28 (1998) 2577–2582.
- [10] K. Yamaguchi, N. Mizuno, *Angew. Chem. Int. Ed.* 41 (2002) 4538–4542.
- [11] K. Yamaguchi, N. Mizuno, *Chem. Eur. J.* 9 (2003) 4353–4361.
- [12] C.M. Ho, W.Y. Yu, C.M. Che, *Angew. Chem. Int. Ed.* 43 (2004) 3303–3307.
- [13] L. Zhang, C. Zhang, H. He, *J. Catal.* 261 (2009) 101–109.
- [14] J. Grunwaldt, M. Caravati, A. Baiker, *J. Phys. Chem. B* 110 (2006) 25586–25589.
- [15] C. Evangelisti, G. Vitulli, E. Schiavi, M. Vitulli, S. Bertozzi, P. Salvadori, L. Bertinetti, G. Martra, *Catal. Lett.* 116 (2007) 57–62.
- [16] L. Xu, C. He, M. Zhu, S. Fang, *Catal. Lett.* 114 (2007) 202–205.
- [17] L. Zhang, X. Wang, B. Tan, U.S. Ozkan, *J. Mol. Catal. A: Chem.* 297 (2009) 26–34.
- [18] S. Kim, S. Ihm, *Ind. Eng. Chem. Res.* 41 (2002) 1967–1972.
- [19] I. Fernandez, N. Khiar, *Chem. Rev.* 103 (2003) 3651–3705.
- [20] M.C. Carreno, *Chem. Rev.* 95 (1995) 1717–1760.
- [21] S. Balakumar, P. Thanasekaran, E. Rajkumar, K. John Adaikalasamy, S. Rajagopal, R. Ramaraj, T. Rajendran, B. Manimaran, K.L. Lu, *Org. Biomol. Chem.* 4 (2006) 352–358.
- [22] E. Rajkumar, S. Rajagopal, *Photochem. Photobiol. Sci.* 7 (2008) 1407–1414.
- [23] A. Chellamani, P. Kulanthaipandi, S. Rajagopal, *J. Org. Chem.* 64 (1999) 2232–2239.
- [24] R. Sevel, S. Rajagopal, C. Srinivasan, N.M.I. Alhaji, A. Chellamani, *J. Org. Chem.* 65 (2000) 3334–3340.
- [25] V.K. Sivasubramanian, M. Ganesan, S. Rajagopal, R. Ramaraj, *J. Org. Chem.* 67 (2002) 1506–1514.
- [26] N.S. Venkataramanan, S. Premisingh, S. Rajagopal, K. Pitchumani, *J. Org. Chem.* 68 (2003) 7460–7470.
- [27] N.S. Venkataramanan, G. Kuppuraj, S. Rajagopal, *Coord. Chem. Rev.* 249 (2005) 1249–1268.
- [28] A. Mary Imelda Jayaseeli, S. Rajagopal, *J. Mol. Catal. A: Chem.* 309 (2009) 103–110.
- [29] B. Sreedhar, P. Radhika, B. Neelima, N. Hebalkar, A.K. Mishra, *Catal. Commun.* 10 (2008) 39–44.
- [30] D.N. Dymbtsev, A.L. Nuzhdin, H. Chun, K.P. Bryliakov, E.P. Talsi, V.P.K. Kim, *Angew. Chem. Int. Ed.* 45 (2006) 916–920.
- [31] O. Vidoni, K. Philippot, C. Amiens, B. Chaudret, O. Balmes, J.O. Malm, J.O. Bovin, F. Senocq, M.J. Casanove, *Angew. Chem. Int. Ed.* 38 (1999) 3736–3738.
- [32] A. Nowicki, V.L. Boulaire, A. Roucouxa, *Adv. Synth. Catal.* 349 (2007) 2326–2330.
- [33] C. Pan, K. Pelzer, K. Philippot, B. Chaudret, F. Dassenoy, P. Lecante, M.-J. Casanove, *J. Am. Chem. Soc.* 123 (2001) 7584–7593.
- [34] M. Zawadzki, J. Okal, *Mater. Res. Bull.* 43 (2008) 3111–3121.
- [35] W. Chen, J.R. Davies, D. Ghosh, M.C. Tong, J.P. Konopelski, S. Chen, *Chem. Mater.* 18 (2006) 5253–5259.
- [36] I. Balint, A. Miyazaki, K. Aika, *J. Catal.* 207 (2002) 66–75.
- [37] I. Balint, A. Miyazaki, K. Aika, *Chem. Commun.* (2002) 630–631.
- [38] A.M. Karim, V. Prasad, G. Mpourmpakis, W.W. Lonergan, A.I. Frenkel, J.G. Chen, D.G. Vlachos, *J. Am. Chem. Soc.* 131 (2009) 12230–12239.
- [39] N. Bedford, C. Dablemont, G. Viau, P. Chupas, V. Petkov, *J. Phys. Chem. C* 111 (2007) 18214–18219.
- [40] J. Okal, *Catal. Commun.* 11 (2010) 508–512.
- [41] S. Lowell, J.E. Shields, M.A. Thomas, M. Thommes, *Characterization of Porous Solids and Powders: Surface Area, Pore Size and Density*, Springer, 2004, ISBN 1402023022.
- [42] J.C. Groen, L.A.A. Peffer, J. Perez-Ramirez, *Micropor. Mesopor. Mater.* 60 (2003) 1–17.
- [43] J. Okal, M. Zawadzki, L. Kepinski, L. Krajczyk, W. Tylus, *Appl. Catal. A: Gen.* 319 (2007) 202–209.
- [44] J.A. Mieth, J.A. Schwarz, *J. Catal.* 118 (1989) 218–226.
- [45] I. Balint, A. Miyazaki, K. Aika, *Chem. Mater.* 13 (2001) 932–938.
- [46] J.R. Regalbuto, A. Navada, S. Shadid, M.L. Bricker, Q. Chen, *J. Catal.* 184 (1999) 335–348.
- [47] E. Bus, J.T. Miller, J.A. van Bokhoven, *J. Phys. Chem. B* 109 (2005) 14581–14587.
- [48] J.G. Goodwin Jr., *J. Catal.* 68 (1981) 227–232.
- [49] B.J. Chen, G. Goodwin Jr., *J. Catal.* 158 (1996) 228–235.
- [50] A. Sayari, H.T. Wang, J.G. Goodwin Jr., *J. Catal.* 93 (1985) 368–374.
- [51] C. Zupanc, A. Hornung, O. Hinrichsen, M. Muhler, *J. Catal.* 209 (2002) 501–514.
- [52] X. Yan, H. Liu, K.Y. Liew, *J. Mater. Chem.* 11 (2001) 3387–3391.
- [53] Y. Zhang, J. Yu, H. Niu, H. Liu, *J. Colloid Interface Sci.* 313 (2007) 503–510.
- [54] R.C. Weast, *CRC Handbook of Chemistry and Physics*, 70th ed., CRC Press, Boca Raton, FL, 1989, D-154.
- [55] C. Bock, C. Paquet, M. Couillard, G.A. Botton, B.R. MacDougall, *J. Am. Chem. Soc.* 126 (2004) 8028–8037.
- [56] N. Dimitratos, J.A.L. Sanchez, S. Meenakshisundaram, J.M. Anthonykutty, G. Brett, A.F. Carley, S.H. Taylor, D.W. Knight, G.J. Hutchings, *Green Chem.* 11 (2009) 1209–1216.
- [57] A. Miyazaki, I. Balint, K. Aika, Y. Nakano, *J. Catal.* 204 (2001) 364–371.
- [58] F. Bonet, K.T. Elhissen, K. Vijaya Sarathy, *Bull. Mater. Sci.* 23 (2000) 165–168.
- [59] T.S. Smith, V.L. Pecoraro, *Inorg. Chem.* 41 (2002) 6754–6760.
- [60] D.H. Koo, M. Kim, S. Chang, *Org. Lett.* 7 (2005) 5015–5018.
- [61] G. Du, J.H. Espenson, *Inorg. Chem.* 44 (2005) 2465–2471.
- [62] K.J. Adaikalasamy, N.S. Venkataramanan, S. Rajagopal, *Tetrahedron* 59 (2003) 3613–3619.
- [63] S. Maksoud, A.B. Daniele, Sorokin, *Green Chem.* 10 (2008) 447–451.
- [64] B.M. Choudary, B. Bharathi, Ch.V. Reddy, M.L. Kantam, *J. Chem. Soc. Perkin Trans. 1* (2002) 2069–2074.
- [65] B. Karimi, M. Ghoreishi-Nezhad, J.H. Clark, *Org. Lett.* 7 (2005) 625–628.
- [66] W. Wang, Y. Xu, D.I.C. Wang, Z. Li, *J. Am. Chem. Soc.* 131 (2009) 12892–12893.
- [67] N. Chakroune, G. Viau, S. Ammar, L. Poul, D. Veautier, M.M. Chehimi, C. Mangeney, F. Villain, F. Fievet, *Langmuir* 21 (2005) 6788–6796.
- [68] T. Tsukatani, H. Fujihara, *Langmuir* 21 (2005) 12093–12095.